Hindawi
Advances in Condensed Matter Physics
Volume 2019, Article ID 2157428, 11 pages
https://doi.org/10.1155/2019/2157428

Research Article

Enhanced Photocatalytic Activity of Vanadium-Doped SnO_2 Nanoparticles in Rhodamine B Degradation

H. Letifi,[1,2] Y. Litaiem,[2] D. Dridi,[2,3] S. Ammar,[1,2] and R. Chtourou[2]

[1]*Unité de Recherche Electrochimie, Matériaux et Environnement (UREME), Faculté des Sciences de Gabès, Université de Gabès, Cité Erriadh, 6072 Gabes, Tunisia*
[2]*Laboratory of Nanomaterials and Systems for Renewable Energies (LaNSER), Research and Technology Center of Energy, Techno-Park Borj-Cedria, Hammam-Lif, Tunis, Tunisia*
[3]*Université de Carthage, Faculté des Sciences de Bizerte, Tunis, Tunisia*

Correspondence should be addressed to Y. Litaiem; yousralitaiem@gmail.com

Received 27 April 2019; Revised 15 June 2019; Accepted 25 July 2019; Published 9 October 2019

Academic Editor: Golam M. Bhuiyan

In this paper, we have reported a novel photocatalytic study of vanadium-doped SnO_2 nanoparticles (SnO_2: V NPs) in rhodamine B degradation. These NPs have been prepared with vanadium concentrations varying from 0% to 4% via the coprecipitation method. Structural, morphological, and optical properties of the prepared nanoparticles have been investigated by X-ray diffraction (XRD), Fourier transform infrared (FTIR) spectroscopy, transmission electron microscope (TEM), and UV-Vis and photoluminescence (PL) spectroscopy. Structural properties showed that both undoped and SnO_2: V NPs exhibited the tetragonal structure, and the average crystal size has been decreased from 20 nm to 10 nm with the increasing doping level of vanadium. Optical studies showed that the absorption edge of SnO_2: V NPs showed a redshift with the increasing vanadium concentration. This redshift leads to the decrease in the optical band gap from 3.25 eV to 2.55 eV. A quenching in luminescence intensity has been observed in SnO_2: V NPs, as compared to the undoped sample. Rhodamine B dye (RhB) has been used to study the photocatalytic degradation of all synthesized NPs. As compared to undoped SnO_2 NPs, the photocatalytic activity of SnO_2: V NPs has been improved. RhB dye was considerably degraded by 95% within 150 min over on the SnO_2: V NPs.

1. Introduction

Nowadays, industries continually release hazardous toxic substances such as organic contaminants into water resources [1]. Therefore, a global effort has been paid to overcome this environmental issue. Photocatalysis plays an important role in the disinfection of water by removing these biological and chemical pollutants from water. In a photocatalytic reaction, an electron-hole pair was generated with the use of a photocatalyst which further creates free radicals. These free radicals break down the aromatic structure of dye molecules [2]. Photocatalysts are activated with light in a number of competing processes that schematically are presented in Figure 1. Steps (1) and (2) show electronic processes of e^- and h^+ active centers on the photocatalyst surface. These processes have to compete with deactivation processes (3) and (4), leading to e^- and h^+ recombination. The increase of the distance toward the surface of the active centers of photogenerated electrons and holes also increases the probability of their recombination. The increase in the photocatalyst surface enhances the catalyst activity because the number of active centers depends on the surface area. In order to hinder the recombination process and to increase the photocatalytic activity, it is important that the semiconductor particles must be small and well-crystallized.

Heterogenous photocatalysts, namely, zinc oxide (ZnO) [3–5], titanium dioxide (TiO_2) [5–8], tungsten trioxide (WO_3) [9], ferric oxide (Fe_2O_3) [10, 11], copper oxide (Cu_2O) [12], and tin dioxide (SnO_2) [13–18], have gained huge interest for environmental applications such as water disinfection, hazardous remediation, and water purification.

Among all mentioned photocatalysts, SnO_2 appears as a promised candidate, thanks to its outstanding and versatile properties such as its strong chemical and physical

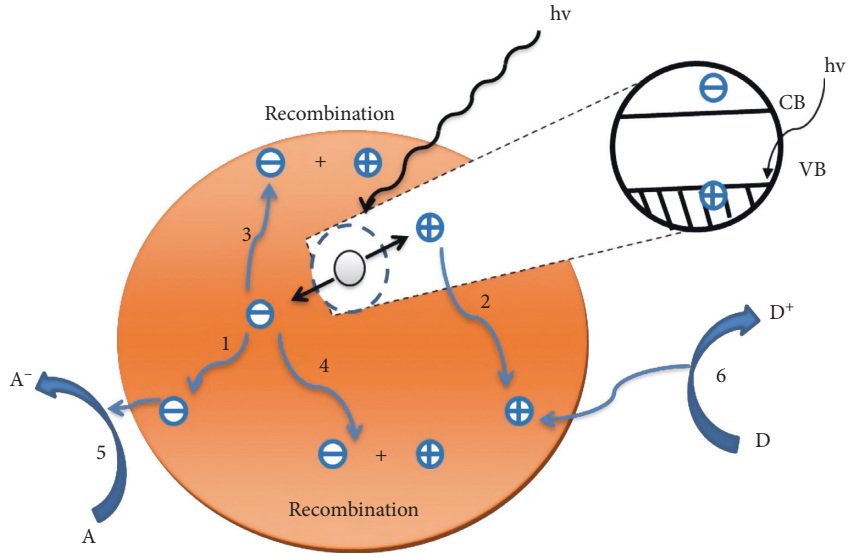

Figure 1: Schematic diagram showing the charge carrier dynamic upon irradiation of a semiconductor. (1) Electron transport to the surface; (2) hole transport to the surface; (3) surface recombination; (4) bulk recombination; (5) electron transfer to an acceptor molecule; (6) hole trapping by a donor molecule.

interaction with absorbed species, high transparency in the visible region, strong thermal stability in air, low operating temperature, wide band gap energy equal to 3.6 [19], chemical and mechanical stability, and high mobility of electrons [20]. These important properties are crucial to make SnO_2 NPs as a practical candidate for various applications, namely, gas sensing [21, 22], optoelectronic devices [23, 24], dye-based solar cells [25], and photocatalytic processes [26].

Thus, SnO_2 NPs have been synthesized using several techniques such as thermal evaporation [27], polyol method [28–30], chemical precipitation [31], sol-gel method [32], hydrothermal method [33, 34], and coprecipitation methods [35, 36]. Among these various methods, the coprecipitation method was chosen in this study, thanks to its important advantages including its low fabrication cost, simplicity, high purity, good reproducibility, and low operation temperature.

So far, several attempts have been conducted on doping SnO_2 NPs with transition metals such as cobalt [37, 38], nickel [39], chromium [40], iron [41], magnesium [42], and vanadium [43], aiming to extend the photo response of SnO_2 from the ultraviolet to the visible region [44]. Moreover, adding amounts of these dopant species can efficiently extend the absorption edge of SnO_2 NPs into the visible region which increases the photocatalytic activity. In contrast, high doping content can create electron-hole recombination sites, and the wide energy band gap hinders this photoactivation [45].

Thus, nanostructured semiconductors can efficiently degrade different organic pollutants under UV light irradiation [46]. The decomposition of organic dyes such as methylene blue (MB) and methyl orange [47–49] in aqueous suspension is used as a probe reaction to investigate the catalytic activity of metal oxide nanomaterials. Many studies have been devoted to the use of nanocomposite or heterojunction catalysts such as ZnO/SnO_2 [50], TiO_2/SnO_2 [46], Fe_2O_3/SnO_2 [51], and V_2O_5/SnO_2 [52]. In literature, there are several works reported on investigating the vanadium-doped SnO_2 nanoparticles SnO_2: V NPs [53] by studying the effect of doping concentration on chemical, physical, and structural properties of nanoparticles of much importance for technological applications. However, few reports have been conducted on evaluating the photocatalytic activity of SnO_2: V NPs. Thus, SnO_2: V NPs are more active as catalysts than pure SnO_2 [54–57]. All these studies have proved the enhanced photocatalytic activity of SnO_2 NPs after doping with vanadium (Table 1).

In this paper, undoped and SnO_2: V NPs have been prepared via the coprecipitation method. Then, a detailed discussion has been conducted on studying the structural, morphological, optical, and photoluminescence properties of SnO_2: V NPs. Finally, the photocatalytic activity of the synthesized samples was investigated in rhodamine B degradation under UV light irradiation.

2. Experimental Details

2.1. Sample Preparation. Synthesis of undoped and SnO_2: V NPs was carried by the coprecipitation method. All of the used materials including tin chloride dihydrate ($SnCl_2$. $2\mathbf{H_2O}$, 99.99%) and ammonium metavanadate (NH_4VO_3, 99.99%) have been used in research grade (Merck Co.). Deionized (DI) water has been used for washing precipitants.

A typical and sample preparation procedure consists first to dissolve 4.23 g of tin chloride dihydrate ($SnCl_2$ $2\mathbf{H_2O}$, 99.99%) in 150 ml deionized water. After that, various amounts of ammonium metavanadate (NH_4VO_3, 99.99%) corresponding to 0, 1, 2, and 4 (mol%) will be added with vigorous agitation stirring for 1 h at a temperature of 80°C. pH solution was adjusted by adding ammonia aqueous

Table 1: Photocatalytic activity of SnO_2: V NPs using different methods.

	Method	Crystallite size (nm)	Dye	Photocatalytic efficiency	Ref.
SnO_2: V NPs	Sol-gel	3	Methylene blue and rhodamine B	5% (mol%) showed better photocatalytic activity	[53]
SnO_2: V NPs	Combustion synthesis method	4.52	Rhodamine B	0.05% (mol%) showed better photocatalytic activity	[55]
SnO_2: V NPs	Polyol method	12.1	Methylene blue	10% (mol%) showed better photocatalytic activity	[56]

solution (28%) to reach a value of about 11 for 4 hours. Centrifugation was used to separate the obtained precipitates. The latter was washed many times with ethanol (C_2H_5OH). Finally, the resulting products were dried 12 hours at 80°C and then were calcined for 4 hours at 600°C.

The photocatalytic activities of undoped and SnO_2: V NPs were evaluated for the degradation of rhodamine B dye (RhB) in aqueous solution under a UV light irradiation. The reaction system includes a 9 W UV Philips Bulb lamp emitting a UV light ($\lambda = 365$ nm) with a measured intensity of 20 W/m^2. In a typical experiment, 50 mg of catalyst was dispersed into 50 mL of aqueous solution of RhB solution. The suspension was stirred for about 30 min at 25°C in dark in order to obtain the adsorption-desorption equilibrium between RhB dye and the photocatalyst. The solution was continuously stirred during the experiments. At given irradiation time intervals, 4 mL of the suspension was collected and then centrifuged (6000 rpm, 10 min) to separate the photocatalyst particles. Finally, under constant continuous stirring, the photodegradation process was investigated under UV light irradiation.

2.2. Characterization Techniques. To evaluate crystalline structure and grain size of the all synthesized samples, the X-ray diffraction (XRD) measurements were conducted through using a Panalytical X'Pert Pro diffractometer with the Cu Kα radiation source ($\lambda = 1.54056$ Å). Morphology studies and grain size distribution of the all nanoparticles were recorded with the transmission electron microscopy (TEM, JEM-200CX). FTIR spectra were recorded by means of thermo Nicolet 670 Nexus spectrophotometer (FTIR) spectrometer. The optical properties were attained using UV-visible spectrophotometer (Shimadzu UV 3101). Photoluminescence (PL) spectra were recorded using Shimadzu RF-5301 spectrophotometer with an excitation source wavelength of 266 nm at room temperature and in the spectral range between 300 and 900 nm. The absorption spectra were monitored with PerkinElmer Lambda UV/Vis 950 spectrophotometer using the quartz cuvette in the range 400 and 800 nm during the photodegradation process.

3. Results and Discussion

3.1. Structural Properties. Figure 2 illustrates the XRD spectra of vanadium-doped SnO_2 nanoparticles. As shown in Figure 2, the peaks of all the prepared samples are well indexed according the standard rutile-like, i.e., cassiterite, crystalline structure (*JCPDS card no 41-1445*). There are no

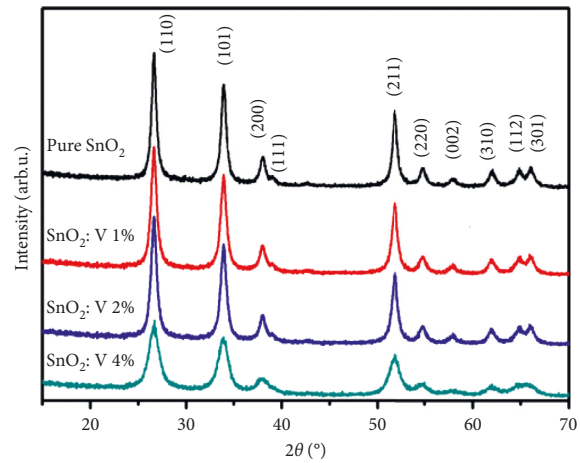

Figure 2: X-ray diffraction of pure SnO_2 and SnO_2: V NPs.

traces neither of vanadium nor of vanadium oxide that can be observed, which illustrates the good crystallinity of the nanoparticles [57]. As compared to the pure SnO_2 NPs, a continuous shift towards higher angle values along with a gradual reduction in the diffraction peak intensity and an expansion of the peak width was observed with the increasing vanadium content.

The average crystallite size **D** and the lattice parameters ($a = b$ and c) for all synthesized samples have been estimated using the Debye–Scherer formula (equation (1)) and equation (2), respectively [58, 59]:

$$\mathbf{D} = \frac{\mathbf{K\lambda}}{\boldsymbol{\beta} \cos \boldsymbol{\theta}}, \tag{1}$$

$$\frac{1}{d^2} = \frac{h^2 + k^2}{a^2} + \frac{l^2}{c^2}, \tag{2}$$

where **D** is the crystalline size (nm), k is a constant related to the crystallite shape (0.9), the X-ray wavelength $\lambda = 1.54056$ Å, $\boldsymbol{\theta}$ is the scattering angle of the reflection identified in the spectra (in radians), $\boldsymbol{\beta}$ is the peak full width at half maximum (FWHM) having the highest intensity (110), d is the interreticular distance, and hkl are the Miller indices. The results are summarized in Table 2.

Consequently, the crystallite sizes have decreased with the increase of vanadium doping concentrations from 19.8 nm for undoped SnO_2 NPs to 10.3 nm for SnO_2: V 4% NPs. Therefore, the density of the SnO_2: V NPs nucleation centers has improved [57, 60]. Moreover, the decrease in lattice constants a and c can be justified by the integration of

Table 2: Crystallographic data (*a* and *c* parameters and volume of the tetragonal unit cell) and average crystallite from XRD of pure SnO_2 and SnO_2: V NPs.

Sample	Position of 2 (°)	*Hkl*	d_{hkl}	$a = b$ (Å)	c (Å)	Average crystallite size (nm) (XRD)	Average crystallite size (nm) (TEM)
	26.54	110	3.354			**19.8**	**21.2**
Pure SnO_2	33.68	101	2.657	4.743	3.207	—	—
	51.69	211	1.766			—	—
	26.57	110	3.350			**17.7**	—
SnO_2: V 1% NPs	33.76	101	2.651	4.736	3.199	—	—
	51.77	210	1.764			—	—
	26.6	110	3.347			**16.8**	—
SnO_2: V 2% NPs	33.81	101	2.648	4.733	3.195	—	—
	51.84	211	1.761			—	—
	26.67	110	3.34			**10.3**	**11.2**
SnO_2: V 4% NPs	33.92	101	2.639	4.723	3.182	—	—
	51.94	211	1.758			—	—

V ions into the SnO_2 lattice and the substitution of Sn sites by vanadium in the form of V^{x+} ($x = 3, 4, 5$), namely, with V^{4+} ($r_V{}^{4+} = 0.63$ Å) or V^{5+} ($r_V{}^{5+} = 0.59$ Å) ions since their ionic radii are smaller than that of Sn^{4+} ($r_{Sn}{}^{4+} = 0.69$ Å) [54, 55].

3.2. Morphological Properties. The TEM images of the pure and SnO_2: V 4% NPs are shown in Figures 3(a) and 3(b), respectively. It can be seen from Figure 3 that the individual particles were nearly spherical in the size in the range of 10 nm–23 nm. The morphologies of the prepared nanoparticles confirm that the grain sizes decrease with the vanadium incorporation into SnO_2 NPs. This result is in well agreement with XRD results. However, a small agglomeration was observed.

3.3. FTIR Analysis. Figure 4 shows the FTIR spectra of pure SnO_2 and SnO_2: V NPs. Generally, the stretching vibrations of Sn-O have been detected between 300 cm^{-1} and 800 cm^{-1} [61]. In our case, the peak observed at 736 cm^{-1} was assigned to the vibration of the Sn-O-Sn bond in SnO_2 lattice. After vanadium incorporation into SnO_2 NPs, a significant new peak located at 935 cm^{-1} for the 2% and 4% vanadium doping contents appeared. The occurrence of this new phase at 935 cm^{-1} may be ascribed to the V-O-Sn bond which can be resulted from the formation of vanadium oxide species. This last result was in agreement with those obtained in [62]. Peaks observed at 1050 cm^{-1} and 1360 cm^{-1} were ascribed to C-O and C-H stretching vibrations, respectively [57]. The hydroxyl groups were observed at 1630 cm^{-1} which is due to the bending vibration of coordinated $\mathbf{H_2O}$ as well as Sn-OH [28, 63]. The basic stretching vibrations of hydroxyl groups (free or bonded) were observed as a broad absorption peak at 3600 cm^{-1}. From this figure, we have noticed a blue shift in distinctive peaks originated from the vanadium incorporation into SnO_2 host lattice [61].

3.4. Optical Properties. Figure 5 shows the absorption spectra of undoped and SnO_2: V NPs at different vanadium doping concentrations. It is obvious from Figure 5 that a sharp absorption edge occurred at around 360 nm. It can be assigned to the intrinsic band gap absorption of SnO_2 [64]. The incorporation of vanadium ions into SnO_2 nanoparticles extends the absorption edge to the visible region. Furthermore, the increase of vanadium doping concentration leads to a substantial red-shift of SnO_2: V NPs absorption. This behavior can be explained by the charge transfer process from the valence band (VB) of SnO_2 to the t_{2g} energy level of vanadium which is located just below the conduction band (CB) [56]. The band-gap energy of undoped and SnO_2: V NPs was determined using the Tauc–Lorentz expression [65]:

$$\boldsymbol{\alpha h\nu} = \mathbf{A}\,(\mathbf{h\nu} - \mathbf{Eg})^{n}, \tag{3}$$

where $\boldsymbol{\alpha}$ represents the absorption coefficient, $\mathbf{h\nu}$ is the photon energy ($\mathbf{h}$ is Planck's constant and $\boldsymbol{\nu}$ is the light frequency), $\mathbf{A}$ is a constant, $\mathbf{Eg}$ is an optical band gap, and n is the parameter according to the nature of the semiconductor [66]. For SnO_2, it possesses direct transition, so the exponent n was chosen 1/2.

The band gap of the undoped and SnO_2: V NPs (Figure 6) was determined by extrapolating the linear portion of $(\boldsymbol{\alpha h\nu})^2$ versus $\mathbf{h\nu}$. The calculated band gap values of all synthesized samples are listed in Table 3. It can be clearly seen that the band gap values decrease from 3.3 eV for pure SnO_2 NPs to 2.6 eV for SnO_2: V 4% NPs.

A significant decrease in $\mathbf{Eg}$ values was observed with the increasing vanadium doping content. The reduce in band gap energy was due from an sp-d exchange among d electrons of the vanadium ions substituted on the tin sites and the s and p band electrons of the SnO_2 matrix [56].

3.5. Photoluminescence Analysis. Figure 7 displays the room temperature PL emission spectra of the SnO_2: V NPs. PL spectra of SnO_2: V NPs exhibited a strong band centered at around 436 nm. The band emission around 436 nm can be attributed to the near-band edge emission (NBE) coming from the holes in the valence band and radiative recombination of electrons in the conduction band [40, 67]. The PL intensity of SnO_2: V NPs has been decreased with increasing vanadium doping content into

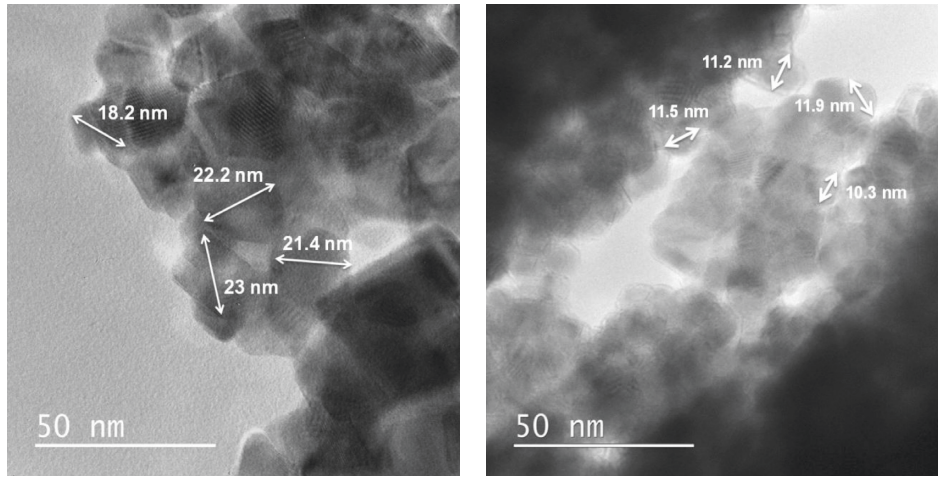

(a) (b)

Figure 3: TEM images of (a) pure SnO_2 and (b) SnO_2: V NPs.

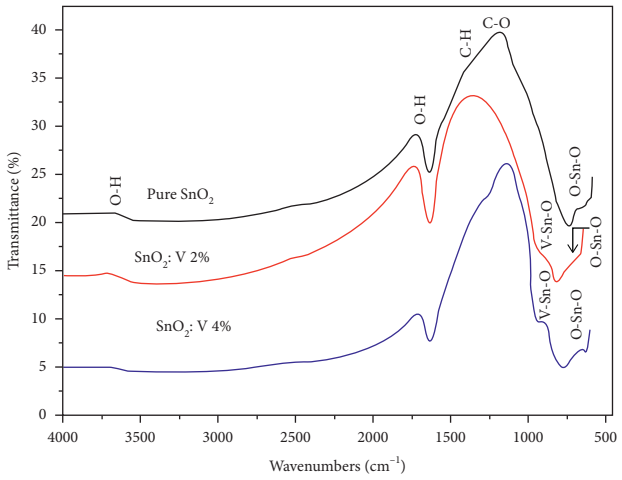

Figure 4: FTIR spectra of pure SnO_2 and SnO_2: V NPs calcined at 600°C.

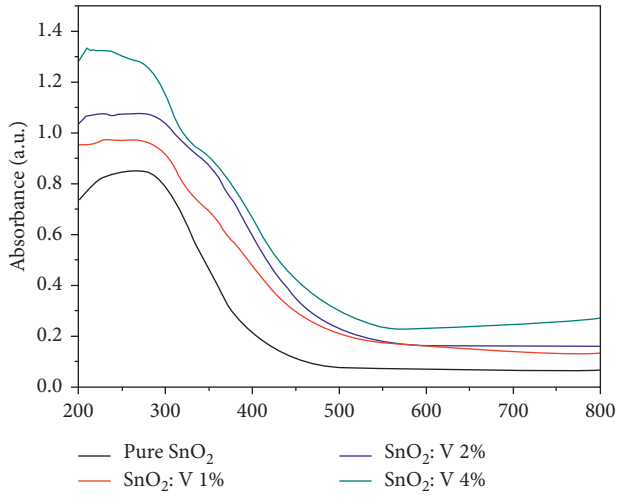

Figure 5: UV-Vis DRS of pure SnO_2 and SnO_2: V NPs with different V doping contents.

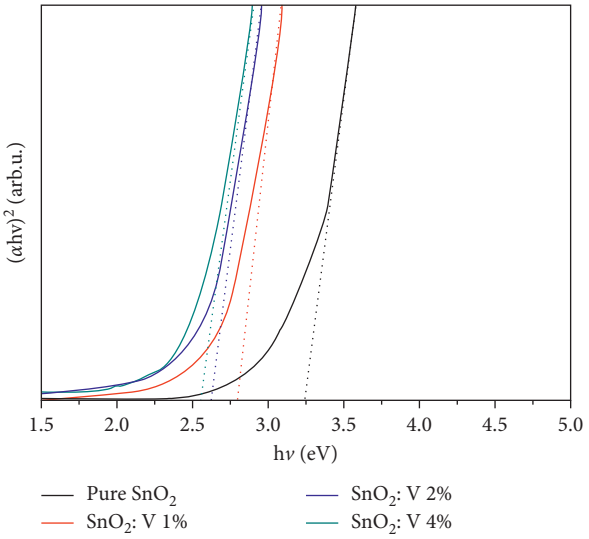

Figure 6: Plots of $(\alpha h\nu)^2$ versus hν of pure SnO_2 and SnO_2: V NPs.

Table 3: Band gap energy and average crystallite size of pure SnO_2 and SnO_2: V NPs.

Samples	Gap energy (eV)	Average crystallite size (nm) (XRD)
Pure SnO_2	**3.25**	**19.8**
SnO_2 :V 1%NPs	**2.80**	**17.7**
SnO_2 :V 2%NPs	**2.63**	**16.8**
SnO_2 :V 4%NPs	**2.55**	**10.3**

SnO_2 nanoparticles. This decrease was attributed to the vanadium doping effect. This enhances the nonradiative recombination of the excited electrons [68]. These results are consistent with those reported in [56, 69].

3.6. Photocatalytic Activity. The photocatalytic activity of the SnO_2: V NPs photocatalysts was carried out by degradation of rhodamine B dye under UV light irradiation by varying

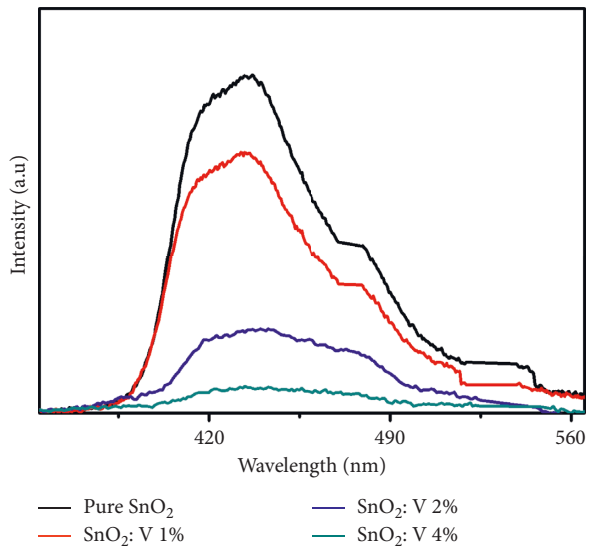

Figure 7: Photoluminescence spectra of pure SnO_2 and SnO_2: V NPs.

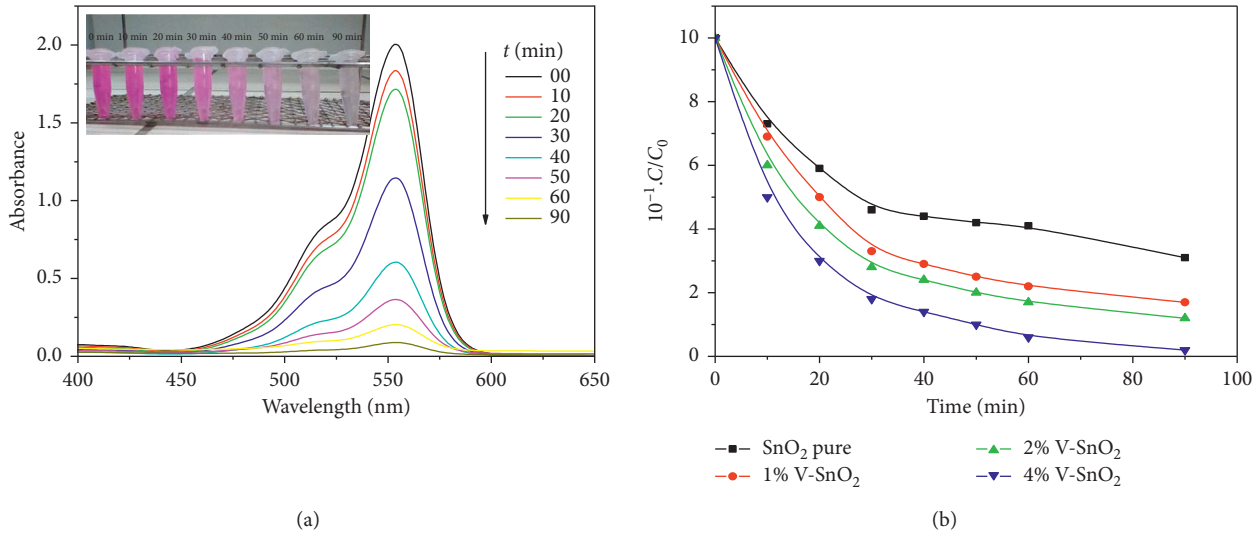

Figure 8: (a) Time-dependent UV-Vis absorbance spectra; (b) photo degradation rate of the rhodamine B pollutant under UV light and light irradiation time.

the exposure time from 0 to 90 min, which is given in Figure 8(a). It can be seen from Figure 8(a) that the intensity of the characteristic peak of RhB dye at around 554 nm was slightly diminished by increasing the exposure time from 0 to 90 min. The optimum time needed for the degradation of RhB dye was about 1 h 30 min. It was noticeable from Figure 8(b) that, after vanadium incorporation into SnO_2 NPs, the photocatalytic activity has been enhanced as compared to undoped photocatalyst. The highest photocatalytic activity was obtained with the SnO_2: V 4% NPs photocatalyst. This result was in agreement with both of the obtained UV-Vis and PL results. The progressive decrease of PL intensity along with band gap values after vanadium incorporation into SnO_2 NPs leads to improve the electron-hole charge separation rate [70]. The highest photocatalytic performance obtained with SnO_2: V 4% NPs resulted from the enhanced charge separation rate at this proper 4% vanadium doping content. These results are similar to those reported in such research works [56, 61, 70–72].

Figure 9 displays the plot of C/C_0 versus irradiation time of SnO_2: V 4% NPs by varying the catalyst amount from 0.1 g to 2 g. A noticed improvement in the degradation rate was achieved by modifying the catalyst quantity from 0.1 g/L to 1.2 g/L. The degradation rate has increased from 51% to 95% which can be attributed to the availability of more active sites on the catalyst surface for adsorption of the dye molecules [73]. Further increase in the catalyst amount up to 2 g/L leads to a slight decrease in the photocatalytic rate from 95% to 85%. This can be ascribed to a reduced light penetration due to the turbidity of the solution [74] or even to the agglomeration of SnO_2 nanoparticles in the reaction system and a reduction in active sites on the catalyst surface, as

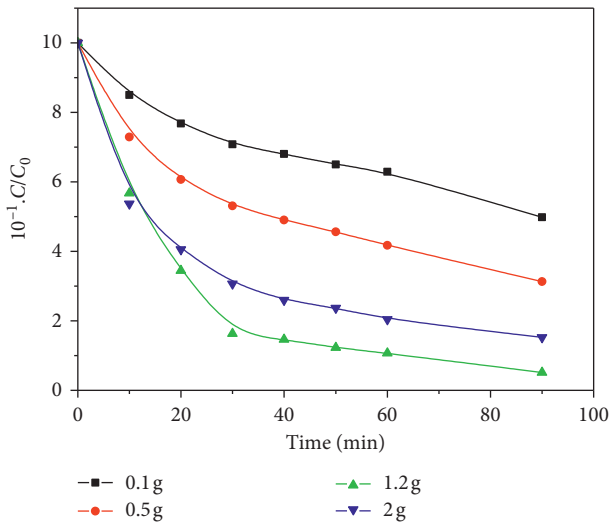

Figure 9: Plot of C/C_0 versus irradiation time of SnO_2: V 4% NPs by varying the catalyst amount from 0.1 g to 2 g.

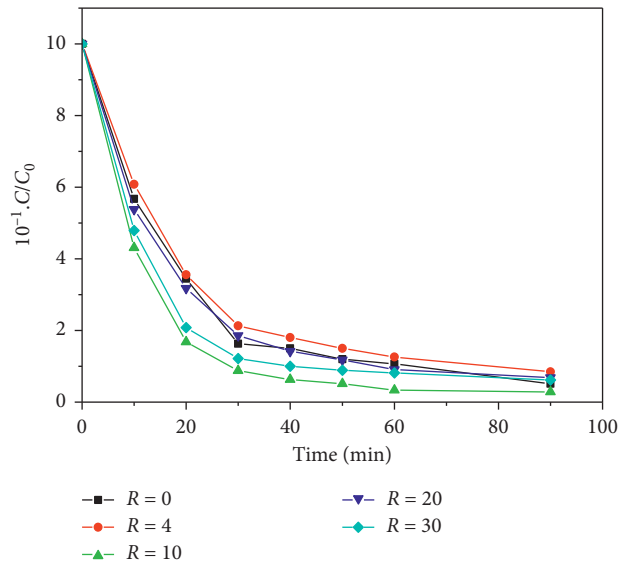

Figure 10: Degradation of the RhB dye for SnO_2: V 4% NPs by varying the molar ratio R of $\mathbf{H_2O_2}$ from 0 to 30.

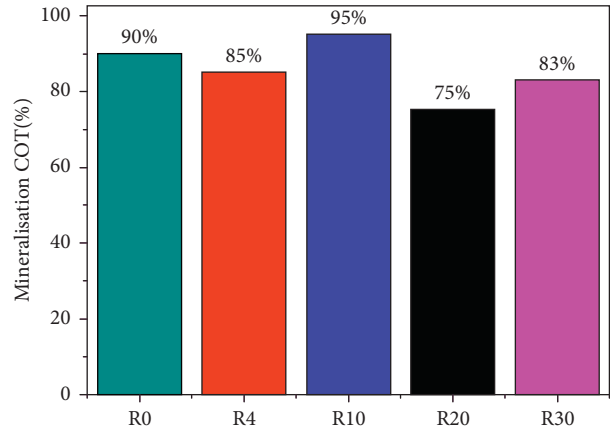

Figure 11: Bar diagram for the % degradation of rhodamine B dye (TOC) in the presence of pure SnO_2 and SnO_2: V NPs.

suggested by B. Babu et al. in [75–77]. Hence, the optimum degradation rate above 95% after 150 minutes of irradiation was achieved by a fixed catalyst quantity equal to 1.2 g/L.

Afterwards, in order to enhance the RhB degradation, hydrogen peroxide ($\mathbf{H_2O_2}$) was added using 1.2 g which is the optimal amount of SnO_2: V 4% catalyst. The degradation of the RhB dye by varying the molar ratio R of $\mathbf{H_2O_2}$ with respect to $(RhB)_0$ from 0 to 30 is shown in Figure 10. It is readily seen that the presence of $\mathbf{H_2O_2}$ inhibited the photocatalytic process with a molar ratio R lying between 20 and 30, while a positive impact of $\mathbf{H_2O_2}$ was noticed for R values in the range between 4 and 10. Additional increase of R beyond 10 contributes to a reduce in the RhB degradation efficiency. It can be related to the increase in the concentration of $\mathbf{OH^{\cdot}}$ radical concentration in the SnO_2: V NPs surface and added to that also to the valence band hole (h^+) oxidative potential leading to organic molecules degradation, as recently reported in [78–80].

However, for high concentrations of hydrogen peroxide $\mathbf{H_2O_2}$, the following reactions took place:

$$\mathbf{H_2O_2 + {}^{\cdot}OH \longrightarrow H_2O + HO_2^{\cdot}} \quad (4)$$

$$\mathbf{HO_2^{\cdot} + {}^{\cdot}OH \longrightarrow H_2O + O_2} \quad (5)$$

It can be noticed from these two reactions that high concentration of $\mathbf{H_2O_2}$ has a negative effect on photodegradation kinetics at the one hand. At another hand, these two reactions yield both of radicals ($\mathbf{OH^{\cdot}}$) and ($\mathbf{HO_2^{\cdot}}$) which are necessary for photodegradation of organic molecules.

Indeed, the reaction of electrons with dissolved oxygen molecules to give superoxide radical anions ($\mathbf{O_2^{-}}$), yielding hydroperoxyl radicals ($\mathbf{HO_2^{\cdot}}$) on protonation and finally $\mathbf{OH^{\cdot}}$ radicals, will be more efficient for the photodegradation [80]. The reactions occurred during this mechanism are as follows:

$$V - SnO_2 + h\nu \longrightarrow V - SnO_2 + e^-_{(CB)} + h^+_{(VB)} \quad (6)$$

$$h^+_{(VB)} + \text{dye} \longrightarrow \text{dye}^{\cdot +} \longrightarrow \text{oxidation of the dye} \quad (7)$$

$$h^+_{(VB)} + \mathbf{H_2O} \longrightarrow \mathbf{H^+ + OH^{\cdot}} \quad (8)$$

$$\mathbf{O_{2(ads)} + e^-_{(CB)} \longrightarrow O_2^{-}} \quad (9)$$

$$\mathbf{O^-_{2(ads)} + H_2O \longrightarrow HO_2^{\cdot} + OH^-} \quad (10)$$

$$\mathbf{HO_2^{\cdot} + H_2O \longrightarrow HO^{\cdot} + H_2O_2} \quad (11)$$

$$\text{dye} + \mathbf{OH^{\cdot}} \longrightarrow \text{degradation products} \quad (12)$$

Aiming to confirm the efficiency of SnO_2: V photocatalyst in the treatment of dangerous pollutants, the mineralization of organic molecules at a fixed molar ratio

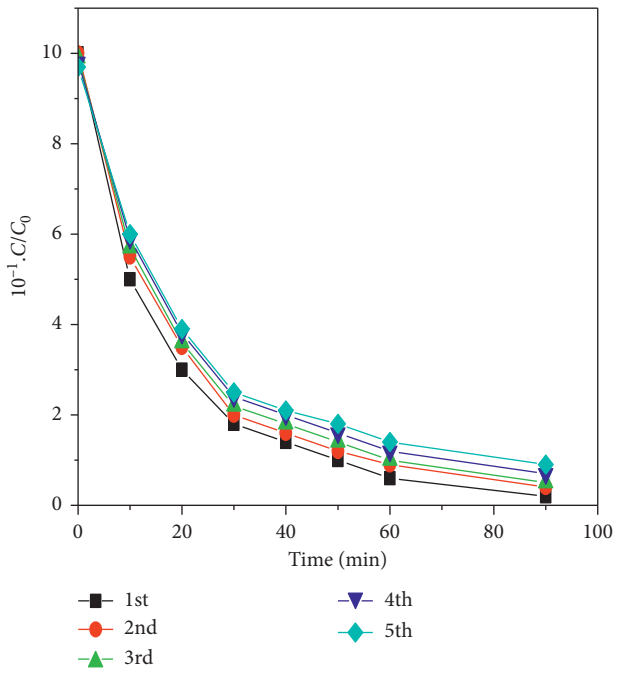

FIGURE 12: Photocatalytic stability of the SnO_2: V 4% NPs sample by the recycle degradation test of rhodamine B with five cycles.

about 10 was evaluated from the total organic carbon (TOC) to be total 100% after 150 min, as shown in Figure 11.

The photocatalytic stability of SnO_2: V NPs was investigated by the recycle degradation test of rhodamine B. The used photocatalysts were washed, dried, and reused in each cycle. As shown in Figure 12, the concentration of RhB varies with respect to time at five cycles. During the repeated experiments, SnO_2: V photocatalysts remain stable enough. It can be concluded that the photocatalysts conserved the same original structure after 5 cycles, and the cycle stability of samples is a result of the stable nanostructure.

4. Conclusion

In this present work, SnO_2: V NPs have been successfully synthesized via the coprecipitation method. XRD patterns showed that the synthesized samples have rutile phases, and the crystallite structure was tetragonal. Lattice parameters values ($a = b$ and c) decreased with the increasing vanadium content, indicating the incorporation of vanadium ions in SnO_2 lattice. Crystallite sizes of the SnO_2: V NPs nanoparticles were obtained from XRD. The same crystallite sizes of SnO_2: V NPs were estimated by TEM. Vanadium incorporation into SnO_2 NPs was proved by FTIR analyses. A red-shift was noticed from UV-Vis spectra of SnO2 : V NPs which can be assigned to a decrease in band gaps from 3.25 eV for pure SnO_2 NPS to 2.55 eV SnO_2: V 4% NPs. Furthermore, the PL intensity increased with the addition of the vanadium amount. The photocatalytic degradation was carried out by using the RhB dye under UV light irradiation of all synthesized SnO_2: V NPs. RhB dye was considerably degraded by 95% within 150 min over on the SnO_2: V NPs. SnO_2: V 4% NPs have the smallest crystallite size estimated from XRD and TEM analyses, the highest band gap energy, and highest photocatalytic activity in RhB degradation.

Data Availability

The data used to support the findings of this study are included within the article.

Conflicts of Interest

All authors declare that there are no conflicts of interest regarding the publication of this paper.

Acknowledgments

This work was funded by the Ministry of Higher Education and Scientific Research of Tunisia.

References

[1] U. G. Akpan and B. H. Hameed, "Parameters affecting the photocatalytic degradation of dyes using TiO_2-based photocatalysts: a review," *Journal of Hazardous Materials*, vol. 170, no. 2-3, pp. 520–529, 2009.

[2] N. Julkapli and S. Bagheri, "Graphene supported heterogeneous catalysts: an overview," *International Journal of Hydrogen Energy*, vol. 40, no. 2, pp. 948–979, 2014.

[3] N. Daneshvar, D. Salari, and A. R. Khataee, "Photocatalytic degradation of azo dye acid red 14 in water on ZnO as an alternative catalyst to TiO_2," *Journal of Photochemistry and Photobiology A: Chemistry*, vol. 162, no. 2-3, pp. 317–322, 2004.

[4] S. Jamil, M. R. S. A. Janjua, S. R. Khan, and N. Jahan, "Synthesis, characterization and catalytic application of polyhedron zinc oxide microparticles," *Materials Research Express*, vol. 4, no. 1, pp. 015902–015910, 2017.

[5] S. Pekárek, J. Mikeš, and J. Krýsa, "Comparative study of TiO_2 and ZnO photocatalysts for the enhancement of ozone generation by surface dielectric barrier discharge in air," *Applied Catalysis A: General*, vol. 502, pp. 122–128, 2015.

[6] A. R. Khataee and M. B. Kasiri, "Photocatalytic degradation of organic dyes in the presence of nanostructured titanium dioxide: influence of the chemical structure of dyes," *Journal of Molecular Catalysis A: Chemical*, vol. 328, no. 1-2, pp. 8–26, 2010.

[7] B. Yao, C. Peng, W. Zhang, Q. Zhang, J. Niu, and J. Zhao, "A novel Fe(III) porphyrin-conjugated TiO_2 visible-light photocatalyst," *Applied Catalysis B: Environmental*, vol. 174-175, pp. 77–84, 2015.

[8] F. Ren, H. Li, Y. Wang, and J. Yang, "Enhanced photocatalytic oxidation of propylene over V-doped TiO_2 photocatalyst: reaction mechanism between V^{5+} and single-electron-trapped oxygen vacancy," *Applied Catalysis B: Environmental*, vol. 176-177, pp. 160–172, 2015.

[9] J. Kim, C. W. Lee, and W. Choi, "Platinized WO_3 as an environmental photocatalyst that generates OH radicals under visible light," *Environmental Science & Technology*, vol. 44, no. 17, pp. 6849–6854, 2010.

[10] S.-W. Cao and Y.-J. Zhu, "Hierarchically nanostructured α-Fe_2O_3 hollow spheres: preparation, growth mechanism, photocatalytic property, and application in water treatment," *The Journal of Physical Chemistry C*, vol. 112, no. 16, pp. 6253–6257, 2008.

[11] S. K. Lakhera, A. Watts, H. Y. Hafeez, and B. Neppolian, "Interparticle double charge transfer mechanism of heterojunction α-Fe_2O_3/Cu_2O mixed oxide catalysts and its visible light photocatalytic activity," *Catalysis Today*, vol. 300, pp. 58–70, 2018.

[12] H. Yang, J. Ouyang, A. Tang et al., "Electrochemical synthesis and photocatalytic property of cuprous oxide nanoparticles," *Materials Research Bulletin*, vol. 41, no. 7, pp. 1310–1318, 2006.

[13] M. U. Khalid, S. R. Khan, and S. Jamil, "Morphologically controlled synthesis of cubes like tin oxide nanoparticles and study of its application as photocatalyst for Congo red degradation and as fuel additive," *Journal of Inorganic and Organometallic Polymers and Materials*, vol. 28, no. 1, pp. 168–176, 2018.

[14] S. R. Khan, M. U. Khalid, S. Jamil, S. Li, A. Mujahid, and M. R. S. A. Janjua, "Photocatalytic degradation of reactive black 5 on the surface of tin oxide microrods," *Journal of Water and Health*, vol. 16, no. 5, pp. 773–781, 2018.

[15] S. Kumar, M. Kumar, A. Thakur, and S. Patial, "Water treatment using photocatalytic and antimicrobial activities of tin oxide nanoparticles," *Indian Journal of Chemical Technology*, vol. 24, pp. 435–440, 2017.

[16] S. P. Kim, M. Y. Choi, and H. C. Choi, "Photocatalytic activity of SnO_2 nanoparticles in methylene blue degradation," *Materials Research Bulletin*, vol. 74, pp. 85–89, 2016.

[17] P. V. Viet, H. T. Nguyen, C. M. Thi, and L. V. Hieu, "The high photocatalytic activity of SnO_2 nanoparticles synthesized by hydrothermal method," *Journal of Nanomaterials*, vol. 2016, Article ID 1957612, 7 pages, 2016.

[18] M. M. Rashad, A. A. Ismail, I. Osama, I. A. Ibrahim, and A.-H. T. Kandil, "Photocatalytic decomposition of dyes using ZnO doped SnO_2 nanoparticles prepared by solvothermal method," *Arabian Journal of Chemistry*, vol. 7, no. 1, pp. 71–77, 2014.

[19] L. Chinnappa, K. Ravichandran, K. Saravanakumar, G. Muruganantham, and B. Sakthivel, "The combined effects of molar concentration of the precursor solution and fluorine doping on the structural and electrical properties of tin oxide films," *Journal of Materials Science: Materials in Electronics*, vol. 22, no. 12, pp. 1827–1834, 2011.

[20] S. Tazikeh, A. Akbari, A. Talebi, and E. Talebi, "Synthesis and characterization of tin oxide nanoparticles via the co-precipitation method," *Materials Science-Poland*, vol. 32, no. 1, pp. 98–101, 2014.

[21] P. Dai, L. Zhang, G. Li, Z. Sun, X. Liu, and M. Wu, "Two-solvent method synthesis of SnO_2 nanoparticles embedded in SBA-15: gas-sensing and photocatalytic properties study," *Materials Research Bulletin*, vol. 50, pp. 440–445, 2014.

[22] W. Zeng, H. Zhang, Y. Li, W. Chen, and Z. Wang, "Hydrothermal synthesis of hierarchical flower-like SnO_2 nanostructures with enhanced ethanol gas sensing properties," *Materials Research Bulletin*, vol. 57, pp. 91–96, 2014.

[23] F. Fang, Y. Zhang, X. Wu, Q. Shao, and Z. Xie, "Electrical and optical properties of nitrogen doped SnO_2 thin films deposited on flexible substrates by magnetron sputtering," *Materials Research Bulletin*, vol. 68, pp. 240–244, 2015.

[24] Y. Mouchaal, A. Enesca, C. Mihoreanu, A. Khelil, and A. Duta, "Tuning the opto-electrical properties of SnO_2 thin films by Ag^{+1} and In^{+3} co-doping," *Materials Science and Engineering: B*, vol. 199, pp. 22–29, 2015.

[25] Y. Zhang, P. Li, X. Xu et al., "SnO_2 films: in-situ template-sacrificial growth and photovoltaic property based on SnO_2/poly (3-hexyl-thiophene) for hybrid solar cell," *Materials Research Bulletin*, vol. 70, pp. 579–583, 2015.

[26] H. Yuan and J. Xu, "Preparation characterization and photocatalytic activity of nanometer SnO_2," *International Journal of Chemical Engineering and Applications*, vol. 1, pp. 3–6, 2010.

[27] Z. R. Dai, J. L. Gole, J. D. Stout, and Z. L. Wang, "Tin oxide nanowires, nanoribbons, and nanotubes," *The Journal of Physical Chemistry B*, vol. 106, no. 6, pp. 1274–1279, 2002.

[28] W. B. Soltan, M. Mbarki, S. Ammar, O. Babot, and T. Toupance, "Textural, structural and electrical properties of SnO_2 nanoparticles prepared by the polyol method," *Journal of Materials Science: Materials in Electronics*, vol. 26, no. 3, pp. 1612–1618, 2015.

[29] R. Bargougui, N. Bouazizi, W. Ben Soltan, A. Gadri, A. Azzouz, and S. Ammar, "Controlled synthesis and electrical conduction properties of anatase TiO_2 nanoparticles via the polyol method," *Applied Physics A*, vol. 122, no. 4, pp. 309–319, 2016.

[30] W. B. Soltan, M. Mbarki, R. Bargougui, S. Ammar, O. Babot, and T. Toupance, "Effect of hydrolysis ratio on structural, optical and electrical properties of SnO_2 nanoparticles synthesized by polyol method," *Optical Materials*, vol. 58, pp. 142–150, 2016.

[31] K. C. Song and Y. Kang, "Preparation of high surface area tin oxide powders by a homogeneous precipitation method," *Materials Letters*, vol. 42, no. 5, pp. 283–289, 2000.

[32] S. V. Manorama, C. V. Gopal Reddy, and V. J. Rao, "Tin dioxide nanoparticles prepared by sol-gel method for an improved hydrogen sulfide sensor," *Nanostructured Materials*, vol. 11, pp. 643–649, 1999.

[33] F. Du, Z. Guo, and G. Li, "Hydrothermal synthesis of SnO_2 hollow microspheres," *Materials Letters*, vol. 59, no. 19-20, pp. 2563–2565, 2005.

[34] G. E. Patil, D. D. Kajale, V. B. Gaikwad, and G. Jain, "Preparation and characterization of SnO_2 nanoparticles by hydrothermal route," *International Nano Letters*, vol. 2, no. 1, p. 17, 2012.

[35] H.-H. Ko, C.-S. Hsi, M.-C. Wang, and X. Zhao, "Crystallite growth kinetics of TiO_2 surface modification with 9mol% ZnO prepared by a coprecipitation process," *Journal of Alloys and Compounds*, vol. 588, pp. 428–439, 2014.

[36] R. Bargougui, A. Oueslati, G. Schmerber et al., "Structural, optical and electrical properties of Zn-doped SnO_2 nanoparticles synthesized by the co-precipitation technique," *Journal of Materials Science: Materials in Electronics*, vol. 25, no. 5, pp. 2066–2071, 2014.

[37] P. Chetri and A. Choudhury, "Investigation of structural and magnetic properties of nanoscale Cu doped SnO_2: an experimental and density functional study," *Journal of Alloys and Compounds*, vol. 627, pp. 261–267, 2015.

[38] B. Babu, C. V. Reddy, J. Shim, R. V. S. S. N. Ravikumar, and J. Park, "Effect of cobalt concentration on morphology of Co-doped SnO_2 nanostructures synthesized by solution combustion method," *Journal of Materials Science: Materials in Electronics*, vol. 27, no. 5, pp. 5197–5203, 2016.

[39] S. Zhuang, X. Xu, Y. Pang, H. Li, B. Yu, and J. Hu, "Variation of structural, optical and magnetic properties with Co-doping in $Sn_{1-x}Co_xO_2$ nanoparticles," *Journal of Magnetism and Magnetic Materials*, vol. 327, pp. 24–27, 2013.

[40] B. Liu, X. Wang, G. Cai, L. Wen, Y. Song, and X. Zhao, "Low temperature fabrication of V-doped TiO_2 nanoparticles, structure and photocatalytic studies," *Journal of Hazardous Materials*, vol. 169, no. 1-3, pp. 1112–1118, 2009.

[41] J. Sakuma, K. Nomura, C. Barrero, and M. Takeda, "Mössbauer studies and magnetic properties of SnO_2 doped

with ^{57}Fe," *Thin Solid Films*, vol. 515, no. 24, pp. 8653–8655, 2007.

[42] S. Wang and H. Y. H. Chen, "Diversity of northern plantations peaks at intermediate management intensity," *Forest Ecology and Management*, vol. 259, no. 3, pp. 360–366, 2010.

[43] D. Toloman, A. Popa, O. Raita et al., "Luminescent properties of vanadium-doped SnO_2 nanoparticles," *Optical Materials*, vol. 37, pp. 223–228, 2014.

[44] S. M. Hassan, A. I. Ahmed, and M. A. Mannaa, "Structural, photocatalytic, biological and catalytic properties of SnO_2/TiO_2 nanoparticles," *Ceramics International*, vol. 44, no. 6, pp. 6201–6211, 2018.

[45] X. Z. Li and F. B. Li, "Study of Au/Au^{3+}-TiO_2 photocatalysts toward visible photooxidation for water and wastewater treatment," *Environmental Science & Technology*, vol. 35, no. 11, pp. 2381–2387, 2001.

[46] M. Huang, J. Yu, B. Li et al., "Intergrowth and coexistence effects of TiO_2–SnO_2 nanocomposite with excellent photocatalytic activity," *Journal of Alloys and Compounds*, vol. 629, pp. 55–61, 2015.

[47] S. M. Hosseinpour-Mashkani and A. Sobhani-Nasab, "Green synthesis and characterization of $NaEuTi_2O_6$ nanoparticles and its photocatalyst application," *Journal of Materials Science: Materials in Electronics*, vol. 28, no. 5, pp. 4345–4350, 2017.

[48] M. Salavati-Niasari, F. Soofivand, A. Sobhani-Nasab, M. Shakouri-Arani, A. Yeganeh Faal, and S. Bagheri, "Synthesis, characterization, and morphological control of $ZnTiO_3$ nanoparticles through sol-gel processes and its photocatalyst application," *Advanced Powder Technology*, vol. 27, no. 5, pp. 2066–2075, 2016.

[49] A. Sobhani-Nasab and M. Behpour, "Synthesis, characterization, and morphological control of Eu2Ti2O7 nanoparticles through green method and its photocatalyst application," *Journal of Materials Science: Materials in Electronics*, vol. 27, no. 11, pp. 11946–11951, 2016.

[50] Z. Zhang, C. Shao, X. Li et al., "Electrospun nanofibers of ZnO–SnO_2 heterojunction with high photocatalytic activity," *The Journal of Physical Chemistry C*, vol. 114, no. 17, pp. 7920–7925, 2010.

[51] C. Zhu, Y. Li, Q. Su et al., "Electrospinning direct preparation of SnO_2/Fe_2O_3 heterojunction nanotubes as an efficient visible-light photocatalyst," *Journal of Alloys and Compounds*, vol. 575, pp. 333–338, 2013.

[52] M. Shahid, I. Shakir, S.-J. Yang, and D. J. Kang, "Facile synthesis of core-shell SnO_2/V_2O_5 nanowires and their efficient photocatalytic property," *Materials Chemistry and Physics*, vol. 124, no. 1, pp. 619–622, 2010.

[53] X. Xue, R. Chen, C. Yan et al., "Review on photocatalytic and electrocatalytic artificial nitrogen fixation for ammonia synthesis at mild conditions: advances, challenges and perspectives," *Nano Research*, vol. 12, no. 6, pp. 1229–1249, 2019.

[54] J. Mazloom, F. E. Ghodsi, and H. Golmojdeh, "Synthesis and characterization of vanadium doped SnO_2 diluted magnetic semiconductor nanoparticles with enhanced photocatalytic activities," *Journal of Alloys and Compounds*, vol. 639, pp. 393–399, 2015.

[55] W. B. Soltan, M. Mbarki, S. Ammar, O. Babot, and T. Toupance, "Structural and optical properties of vanadium doped SnO_2 nanoparticles synthesized by the polyol method," *Optical Materials*, vol. 54, pp. 139–146, 2016.

[56] C. V. Reddy, B. Babu, S. V. P. Vattikuti, R. V. S. S. N. Ravikumar, and J. Shim, "Structural and optical properties of vanadium doped SnO_2 nanoparticles with high photocatalytic activities," *Journal of Luminescence*, vol. 179, pp. 26–34, 2016.

[57] W. B. Soltan, S. Nasri, M. S. Lassoued, and S. Ammar, "Structural, optical properties, impedance spectroscopy studies and electrical conductivity of SnO_2 nanoparticles prepared by polyol method," *Journal of Materials Science: Materials in Electronics*, vol. 28, no. 9, pp. 6649–6656, 2017.

[58] D. Dridi, L. Bouaziz, M. Karyaoui, Y. Litaiem, and R. Chtourou, "Effect of silver doping on optical and electrochemical properties of ZnO photoanode," *Journal of Materials Science: Materials in Electronics*, vol. 29, no. 10, pp. 8267–8278, 2018.

[59] H. P. Klug and L. E. Alexander, *X-Ray Diffraction Procedures for Polycrystalline and Amorphous Materials*, Wiley, New York, NY, USA, 1974.

[60] C.-T. Wang, M.-T. Chen, and D.-L. Lai, "Surface characterization and reactivity of vanadium-tin oxide nanoparticles," *Applied Surface Science*, vol. 257, no. 11, pp. 5109–5114, 2011.

[61] C. V. Reddy, B. Babu, and J. Shim, "Synthesis of Cr-doped SnO_2 quantum dots and its enhanced photocatalytic activity," *Materials Science and Engineering B*, vol. 223, pp. 131–142, 2017.

[62] C.-T. Wang and M.-T. Chen, "Vanadium-promoted tin oxide semiconductor carbon monoxide gas sensors," *Sensors and Actuators B: Chemical*, vol. 150, no. 1, pp. 360–366, 2010.

[63] S. N. Pusawale, P. R. Deshmukh, and C. D. Lokhande, "Chemical synthesis of nanocrystalline SnO_2 thin films for supercapacitor application," *Applied Surface Science*, vol. 257, no. 22, pp. 9498–9502, 2011.

[64] M. T. Uddin, Y. Nicolas, C. Olivier et al., "Nanostructured SnO_2-ZnO heterojunction photocatalysts showing enhanced photocatalytic activity for the degradation of organic dyes," *Inorganic Chemistry*, vol. 51, no. 14, pp. 7764–7773, 2012.

[65] D. Dridi, Y. Litaiem, M. Karyaoui, and R. Chtourou, "Correlation between photoelectrochemical and photoluminescence measurements of Ag-doped ZnO/ITO photoanode," *The European Physical Journal Applied Physics*, vol. 85, no. 2, p. 20401, 2019.

[66] A. N. Banerjee and K. K. Chattopadhyay, "Size-dependent optical properties of sputter-deposited nanocrystalline p-type transparent $CuAlO_2$ thin films," *Journal of Applied Physics*, vol. 97, no. 8, Article ID 084308, 2005.

[67] T. Krishnakumar, R. Jayaprakash, M. Parthibavarman, A. R. Phani, V. N. Singh, and B. R. Mehta, "Microwave-assisted synthesis and investigation of SnO_2 nanoparticles," *Materials Letters*, vol. 63, no. 11, pp. 896–898, 2009.

[68] H. Tang, H. Berger, P. E. Schmid, F. Lévy, and G. Burri, "Photoluminescence in TiO_2 anatase single crystals," *Solid State Communications*, vol. 87, no. 9, pp. 847–850, 1993.

[69] H. Mansour, R. Bargougui, A. Gadri, and S. Ammar, "Co-precipitation synthesis of V-doped titania: influence of vanadium concentration on the structural and optical properties," *Journal of Materials Science: Materials in Electronics*, vol. 28, no. 2, pp. 1852–1858, 2017.

[70] B. Babu, A. N. Kadam, G. T. Rao, S.-W. Lee, C. Byon, and J. Shim, "Enhancement of visible-light-driven photoresponse of Mn-doped SnO_2 quantum dots obtained by rapid and energy efficient synthesis," *Journal of Luminescence*, vol. 195, pp. 283–289, 2018.

[71] K. Nagaveni, M. S. Hegde, and G. Madras, "Structure and photocatalytic activity of $Ti_{1-x}M_xO_{2\pm\delta}$ (M = W, V, Ce, Zr, Fe, and Cu) synthesized by solution combustion method," *The Journal of Physical Chemistry B*, vol. 108, no. 52, pp. 20204–20212, 2004.

[72] J. Liqiang, Q. Yichun, W. Baiqi et al., "Review of photoluminescence performance of nano-sized semiconductor materials and its relationships with photocatalytic activity," *Solar Energy Materials and Solar Cells*, vol. 90, no. 12, pp. 1773–1787, 2006.

[73] S. K. Kansal, A. Hassan Ali, and S. Kapoor, "Photocatalytic decolorization of biebrich scarlet dye in aqueous phase using different nanophotocatalysts," *Desalination*, vol. 259, no. 1-3, pp. 147–155, 2010.

[74] K. Vignesh, A. Suganthi, M. Rajarajan, and S. A. Sara, "Photocatalytic activity of AgI sensitized ZnO nanoparticles under visible light irradiation," *Powder Technology*, vol. 224, pp. 331–337, 2012.

[75] B. Babu, R. Koutavarapu, V. V. N. Harish, J. Shim, and K. Yoo, "Novel in-situ synthesis of Au/SnO_2 quantum dots for enhanced visible-light-driven photocatalytic applications," *Ceramics International*, vol. 45, no. 5, pp. 5743–5750, 2019.

[76] W. B. Soltan, S. Ammar, C. Olivier, and T. Toupance, "Influence of zinc doping on the photocatalytic activity of nanocrystalline SnO_2 particles synthesized by the polyol method for enhanced degradation of organic dyes," *Journal of Alloys and Compounds*, vol. 729, pp. 638–647, 2017.

[77] R. Malik, V. K. Tomer, P. S. Rana, S. P. Nehra, and S. Duhan, "Surfactant assisted hydrothermal synthesis of porous 3-D hierarchical SnO_2 nanoflowers for photocatalytic degradation of Rose Bengal," *Materials Letters*, vol. 154, pp. 124–127, 2015.

[78] Y. Cong, J. Zhang, F. Chen, and M. Anpo, "Synthesis and characterization of nitrogen-doped TiO_2 nanophotocatalyst with high visible light activity," *The Journal of Physical Chemistry C*, vol. 111, no. 19, pp. 6976–6982, 2007.

[79] R. Dholam, N. Patel, and A. Miotello, "Efficient H_2 production by water-splitting using indium-tin-oxide/V-doped TiO_2 multilayer thin film photocatalyst," *International Journal of Hydrogen Energy*, vol. 36, no. 11, pp. 6519–6528, 2011.

[80] B. Babu, V. V. N. Harish, R. Koutavarapu, J. Shim, and K. Yoo, "Enhanced visible-light-active photocatalytic performance using CdS nanorods decorated with colloidal SnO_2 quantum dots: optimization of core-shell nanostructure," *Journal of Industrial and Engineering Chemistry*, vol. 76, pp. 476–487, 2019.